Potentials of the Thermal Airborne Spectrographic Imager for Environmental Studies

Luca Pipia, Fernando Pérez, Anna Tardà, Vicenç Palà and Roman Arbiol
Institut Cartogràfic de Catalunya (ICC)
Remote Sensing Area
Parc de Montjuïc s/n
08038 Barcelona (Spain)
{luca.pipia, fernando.perez, anna.tarda, vicenc.pala, roman.arbiol}@icc.cat

Keywords: Hyperspectral Remote Sensing, TASI, radiometric calibration, atmospheric correction.

Abstract:

The Thermal Airborne Spectrographic Imager (TASI) is a hyperspectral infrared pushbroom sensor manufactured by the Canadian company ITRES© and operated by the Institut Cartogràfic de Catalunya (ICC) since November 2009. In this work, a brief description of TASI's spectral properties and acquisition process is first provided. The basic steps of the hyperspectral technique employed for the retrieval of pixels' absolute temperature and emissivity spectrum are also outlined. Afterwards, two different types of scenarios are considered to demonstrate TASI's potentials for a wide set of environmental monitoring applications. Diurnal and nocturnal flights with TASI over the city of Barcelona are used to stress the different hyperspectral behavior that an urban environment may present in time. The temperature estimation provided by TASI is assessed using measurements from XEMA stations spread over Barcelona. A study concerning the detection of urban heat-island effects is also undertaken. TASI high-resolution acquisitions in Ebro River's mouth are also analyzed for the retrieval of temperature and emissivity information over natural surfaces.

1- TASI Hyperspectral Sensor

The Thermal Airborne Spectrographic Imager (TASI) by ITRES© is a pushbroom hyperspectral sensor with a 40º Field-Of-View (FOV) operating in the thermal infrared (TIR) spectral region. It nominally acquires 32 bands to provide continuous spectral coverage in the wavelength range 8-11.5µm (Itres, 2010). Thermal IR photons emitted from the scene are focused on a plane through two curved slits, generating hyperspectral images with 640 across-track pixels with 6% overlapping. The number of frames read out is fixed to 200 per second (frame time 5ms), whereas the integration time of the thermal energy ranges from 0.01 to about 2 ms.
Actually, TASI acquires radiance information in 55-bands ranging from 6.5µm up to 12µm, approximately. Bands at the shorter wavelengths are employed to estimate pixels' spectral shift induced by temperature variation within the airborne platform. Remaining bands are radiometrically calibrated, spectrally aligned and filtered in space or frequency by user as needed for blinking pixels removal. At the end of the ITRES traceable processing chain, 32-band hyperspectral data at the system nominal wavelengths (reported in Table 1) are provided.

Channel #	λ_0 [nm]	**Channel #**	λ_0 [nm]	**Channel #**	λ_0[nm]	**Channel #**	λ_0[nm]
1	8000	9	8904	17	9808	25	10712
2	8113	10	9017	18	9921	26	10825
3	8226	11	9130	19	10034	27	10938
4	8339	12	9243	20	10147	28	11051
5	8452	13	9356	21	10260	29	11164
6	8565	14	9469	22	10373	30	11277
7	8678	15	9582	23	10486	31	11390
8	8791	18	9695	24	10599	32	11503

Table 1: Nominal central wavelengths for the filters providing the 32-band TASI data. The nominal bandwidth of all filters is $\Delta\lambda$=110nm.

Radiometric calibration residual errors caused by a 2% uncertainty on the emissivity of the calibration blackbody used are compensated for by an additional post-processing correction block developed at ICC. Using in-lab TASI acquisitions of tap-water at different thermodynamic temperatures, a set of hyperspectral calibration polynomials is estimated for each pixel of the FOV and applied to correct radiance information. After the post-processing calibration step, the accuracy in the retrieval of the absolute temperature information from each channel of the TASI sensor becomes lower than the 0.2 K NEΔT, consistent with the precision claimed by ITRES©[1].

2- Temperature and Emissivity Retrieval

The radiance $L^S(\lambda)$ measured at sensor level is generally factorized as

$$L^S(\lambda)= [L^{\downarrow}(\lambda)\,(1-\varepsilon(\lambda))+ \varepsilon(\lambda)B(T,\lambda)]\tau(\lambda)+ L^{\uparrow}(\lambda), \quad (1)$$

where $B(T,\lambda)$ is the *Planck* function for the spectral radiance, $\varepsilon(\lambda)$ is the unknown surface emissivity and T is the unknown surface or skin temperature, $\tau(\lambda)$ is the atmospheric transmissivity, $L^{\downarrow}(\lambda)$ and $L^{\uparrow}(\lambda)$ and the atmospheric downwelling and upwelling radiance contributions, respectively. In order to separate the emissivity and temperature information coupled in TASI data as shown by (1), the Remote Sensing Group of ICC developed a processing chain based on the technique proposed for the first time in [2] and later modified in [3].

The first step is tackling the problem of estimating the thermal contribution from the atmosphere. To do this, geometrical parameters such as terrain height h, observation angle θ and vertical distance to the sensor Δh are characterized at pixel level. The three parameters are calculated using the Digital-Elevation-Model of the flown area and the trajectory of the airborne platform during the acquisition process. In order to reduce the computational burden, pixels are grouped into subsets using a minimum height increment Δh and a minim angular step $\Delta\theta$. The number of angular sectors $N_\theta = \theta_{max}/\Delta\theta$ and height intervals $N_h = h_{max}- h_{min}/\Delta h$ are then used as input to a ModTran-based simulation block. It is worth pointing out that θ_{max} is fixed to 30º (>FOV/2) to take into account turbulence effects. Essentially, ModTran5.0 [4] is employed to estimate atmospheric downwelling radiance $L^{\downarrow}(\lambda)$, upwelling radiance $L^{\uparrow}(\lambda)$ and transmissivity $\tau(\lambda)$ profiles for the $N_\theta \times N_h$ possible geometries in the thermal infrared spectrum. Then, the spectral properties of FOV's pixels are matched to the corresponding observation geometry, which slightly changes at each line of the hyperspectral image.

The second step is the separation of emissivity $\varepsilon(\lambda)$ and temperature T information. To cope with this issue, the *Automatic Retrieval of Temperature and EMIssivity* using *Spectral Smoothness* (ARTEMISS) algorithm is employed. The rationale of ARTEMISS is that thermal-infrared spectra of solids are much smoother than gases' so that the actual temperature of a pixel is obtained by maximizing the smoothness of emissivity profile $\varepsilon(\lambda)$ [2]. It is plain that the higher the number of channels, the better the accuracy of the retrieved emissivity profile. Concerning the TASI acquisition, it was observed that this approach usually lead to overestimate pixel temperature, and consequently to underestimate pixels' emissivity. Contrarily, the modified formulation of ARTEMISS proposed in [3] led to better results. By defining a starting emissivity usually equal to ε_{ref}=0.95, a reference temperature T_{ref} is obtained at pixel level as

$$T_{ref}=B^{-1}\{[\,L^S(\lambda_T)/\underline{\tau}(\lambda_T)- \underline{L}^{\downarrow}(\,\lambda_T)/\underline{\tau}(\lambda_T)-\underline{L}^{\downarrow}(\,\lambda_T)\,(1-\varepsilon_{ref})]/\varepsilon_{ref},\,\lambda_T\,)\} \quad (2)$$

where the underlined terms are the atmospheric contributions estimated by ModTran5.0, B^{-1} is the inverse Planck function and λ_T is a TASI spectral band where atmosphere is highly transmissive. Then, T_{ref} is used as input seed to an iterative function fitting the measured and estimated radiances. Pixels' temperature T_{opt} is finally estimated as follows

$$T_{opt}=\min[\sigma\{L^S(\lambda)- \underline{L}^S(\lambda,T,\underline{\varepsilon}_{opt})\}] \quad (3)$$

where

$$\underline{L}^S(\lambda) = [(1-\underline{\varepsilon}_{opt}(\lambda))\,\underline{L}^{\downarrow}(\lambda)+\underline{\varepsilon}_{opt}(\lambda)B(T_{opt},\lambda)]\cdot\underline{\tau}(\lambda)+\underline{L}^{\uparrow}(\lambda)] \quad (4)$$

and $\underline{\varepsilon}_{opt}$ is the low-pass filtered emissivity profile obtained for T_{opt}. A 3-sample window is employed operatively for $\underline{\varepsilon}_{opt}$ estimation.

3- Urban Environment Study

Urban areas tend to experience a relatively higher temperature compared with the surrounding rural areas. This thermal difference, in conjunction with waste heat released from urban houses, transportation and industry, contribute to the development of urban heat island (UHI) [5]. In order to look into the temporal evolution of urban environment thermal response, diurnal and nocturnal TASI hyperspectral data were acquired over the city of Barcelona on 10-11 September 2010. Details about the flights are reported in Table 2. The correction for the atmospheric contributions to the hyperspectral radiance measured by TASI was carried out as described in Section 2. To achieve a more reliable description of the atmospheric profile during the acquisition process, the radiosounding data which are daily collected at noon and at midnight by the Servei Meteorològic de Catalunya (*Meteocat*) in Barcelona for weather forecasts were used as input to ModTran5.0 simulator. Then, *ARTEMISS* minimization described in (3) was employed for the retrieval of pixels' absolute temperature.

The two temperature mosaics covering the whole city of Barcelona obtained from the nocturnal and diurnal hyperspectral images are shown in Figure 1 and Figure 2, respectively. Remarkable changes in the thermal behavior of the urban environment are mainly detectable in industrial areas, whose temperature lies in the extreme of the dynamic range of the two images of Barcelona, as well as in rural zones.

In the first case, the roofs of warehouses usually contain a significant amount of metallic parts characterized by low thermal inertia. This fact makes their temperature increase up to values close to 70ºC during the maximum

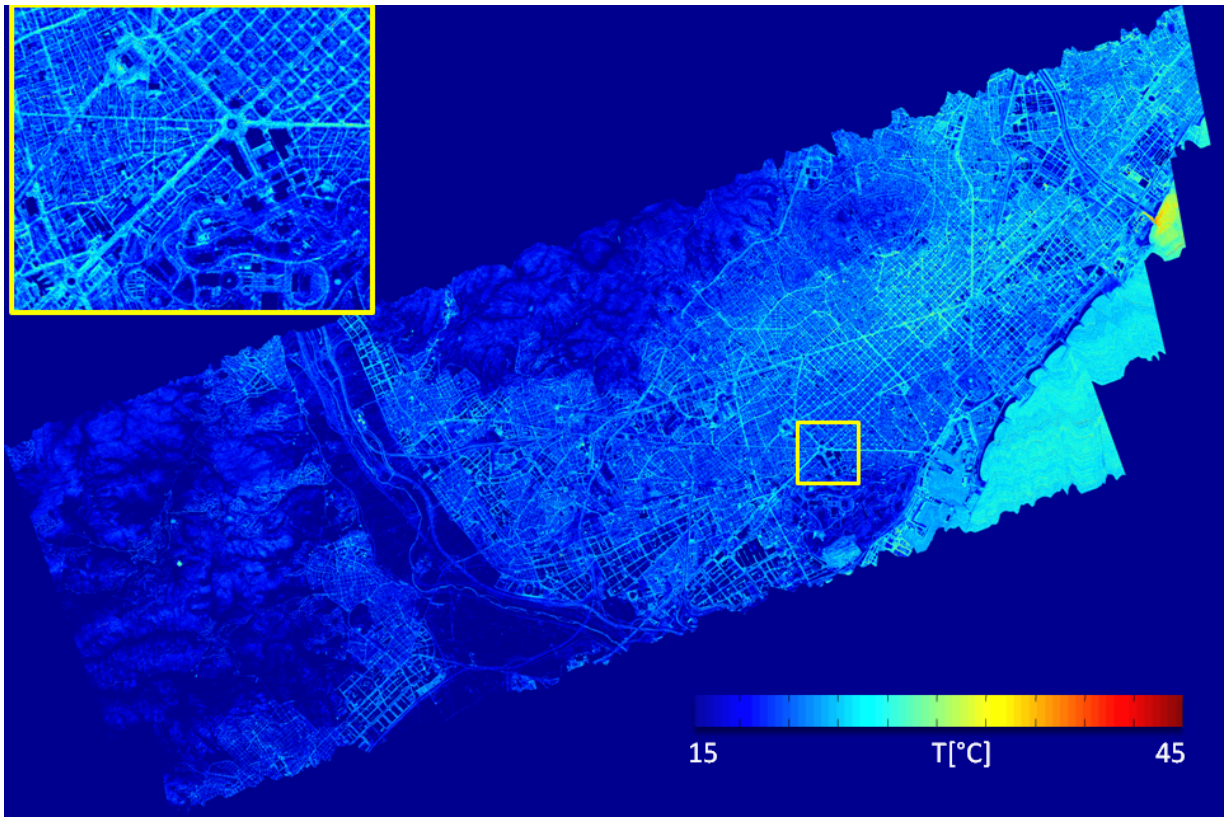

Figure 1: Mosaic of temperature maps retrieved from nocturnal TASI hyperspectral data sets over Barcelona acquired on 10 September 2010.

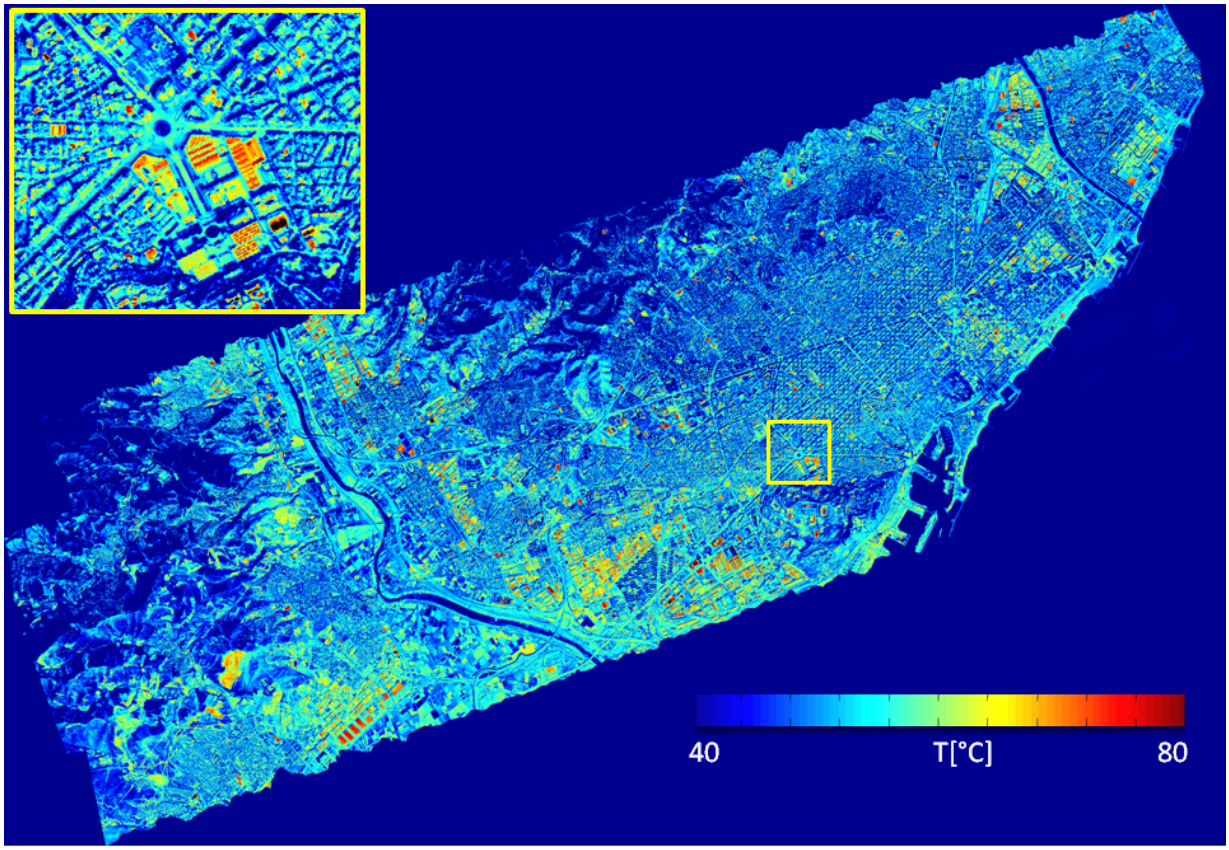

Figure 2: Mosaic of temperature maps retrieved from diurnal TASI hyperspectral data sets over Barcelona acquired on 10 September 2010.

Day	Acquisitions	Time	Pixel Resolution	Integration Time
10/09/2010	BLL09_P1n_T005_f05	23:16	4m × 4m	0.26
10/09/2010	BLL07_P1n_T005_f06	23:27	4m × 4m	0.26
10/09/2010	BLL05_P1n_T005_f08	23:38	4m × 4m	0.26
10/09/2010	BLL08_P1p_T005_f07	23:49	4m × 4m	0.26
11/09/2010	BLL07_P1n_T006_f05	10:31	4m × 4m	0.24
11/09/2010	BLL08_P1p_T006_f06	10:41	4m × 4m	0.24
11/09/2010	BLL06_P1n_T006_f07	10:51	4m × 4m	0.24
11/09/2010	BLL05_P1p_T006_f08	11:05	4m × 4m	0.31

Table 2: Set of diurnal and nocturnal TASI acquisitions over Barcelona in September 2010.

Station	X-UTM [m]	Y-UTM [m]	T Sampling	Sensor Height [m] ASL
Raval	430501	4581904	<60 min>	33
Observatori Fabra	426880	4585800	<30 min>	411
Zoo	432246	4582511	<60 min>	7
Zona Universitaria	425294	4581440	<30 min>	79

Table 3: Details of the four automatic meteorological stations belonging to the XEMA network in Barcelona used for TASI temperature estimation assessment.

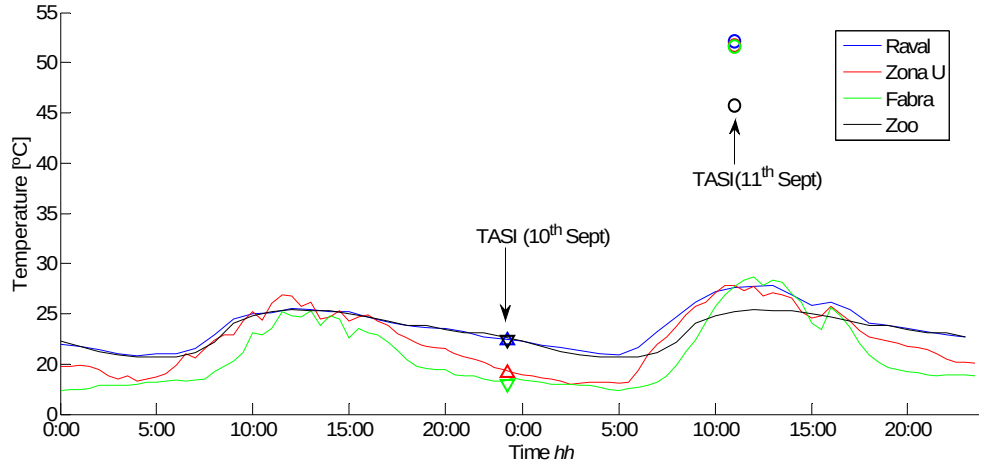

Figure 3: Air temperature evolution in time during the two days of measurements with TASI provided by the four XEMA stations in Barcelona versus TASI-based temperature retrieval.

solar irradiation and decrease down to the value of the coldest pixels within the image during the night. In the second case, non-irrigated, bare or low-vegetated soils are characterized by high thermal excursions during the night-day cycle, being unable to compensate for solar irradiation by evaporation processes due to the low water-content. In Figure 1 it can be also observed the presence of a clear temperature gradient in the delta of the Besós river, north of Barcelona. The water plume is caused by the mixing of the fresh water, colder than sea water, with the hot water produced by the Sant Adrià del Besós thermal power station at the end of the energy generation process and poured into the river just a few meters before the delta. Although the dynamic range used for the diurnal temperature mosaic filters out sea water patterns, it is worth pointing out that the effects of the plume are less noteworthy during the day because the solar irradiation reduces the gap between river and sea skin temperatures.

In order to assess the meaningfulness of using TASI acquisitions for the study of Urban Heat Island (UHIs), the measurements of four meteorological stations belonging to the XEMA [6] (Automatic Weather Station Network, Catalan Meteorological Service-SMC) network and located in different areas of Barcelona were employed. Details concerning the location of the four stations and the temperature time-sampling are available in Table 3. The plots in Figure 3 show the air-temperature time evolution during the two days when data were acquired and also the TASI-based instantaneous estimation . A very good matching between the direct and indirect temperature measurements can be observed for the four XEMA stations during the night. On the contrary, the diurnal case is characterized by the presence of a clear offset between XEMA- and TASI-based estimations. These results agree with the analysis presented in [5], where it is stressed that the detection Urban Heat Islands (UHI) through the observation of Surface Urban Heat Islands (SUHI) requires modeling carefully the interaction between the two layers unless a local thermodynamic equilibrium is assumable. According to the results of the two works, this condition seems to be fulfilled only during the night.

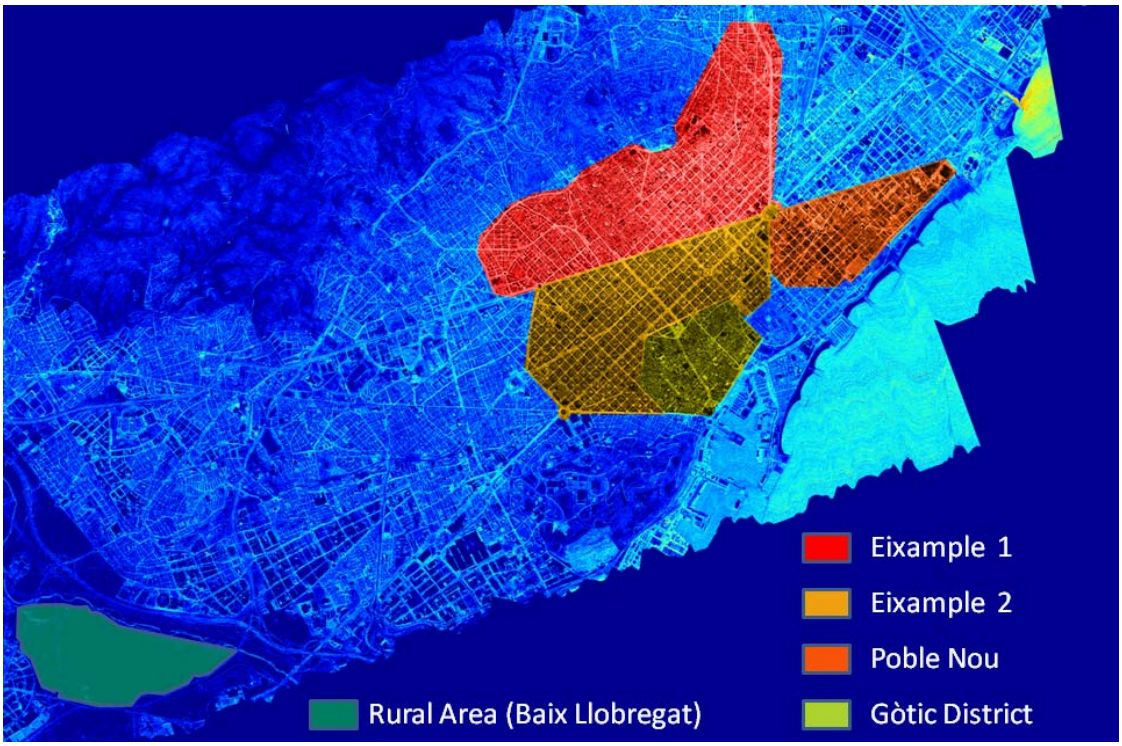

Figure 4: Urban and rural areas selection in Barcelona for the study of Surface Urban Heat Island phenomenon.

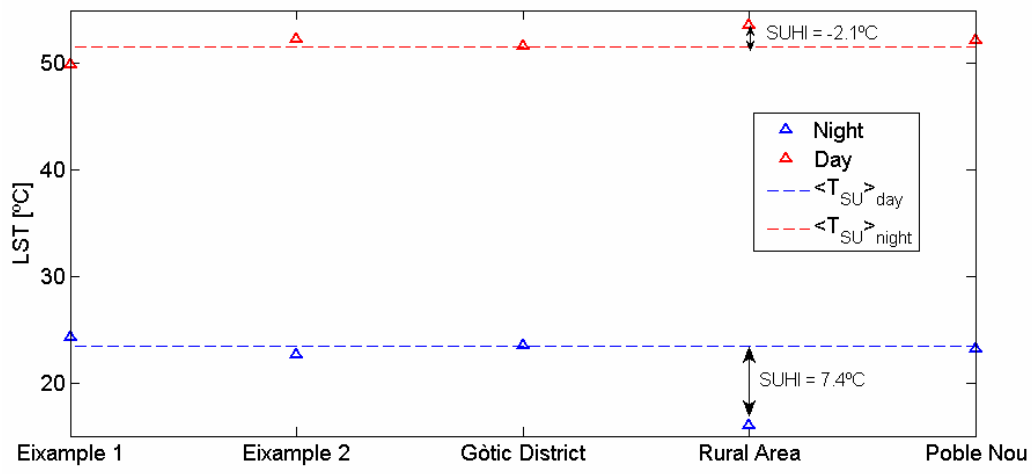

Figure 5: Diurnal and nocturnal distribution of the TASI-based temperature averaged over the urban and rural areas in Barcelona.

Therefore, the study was focused on the presence of SHUIs. An operative equation that is generally employed for the detection of this SHUI phenomenon is [7]

$$SUHI = T_{SU} - T_{SR} \tag{5}$$

where T_{SU} and T_{SR} describe the mean skin-temperature of two areas selected within and outside the city and labeled as urban and rural, respectively. Accordingly, four urban zones within Barcelona and a rural area in the outskirts of the city were identified for the application of (5). A pictorial description of the selection is given in Figure 4. It is worth stressing that the whole area considered for this study is pretty flat so that no temperature change is assumed to be induced by topographic component.

The temperature information retrieved through the application of ARTEMISS to the diurnal and nocturnal collections of TASI data was averaged over the different areas of interest identified in Figure 4. During the night, the mean temperate kept pretty constant over the whole city of Barcelona but a significant drop was observed when leaving the urbanized area. A temperature gap around 7 K was found between the four Barcelona districts and the Baix Llobregat, stressing the presence of SUHI phenomenon. During the day a different behavior was observed, being the rural area characterized by a slightly higher temperature than the mean value of the four urban areas, around 2 K. The results, in agreement with the conclusions drawn in [5], are summarized in the plots of Figure 5.

(a)

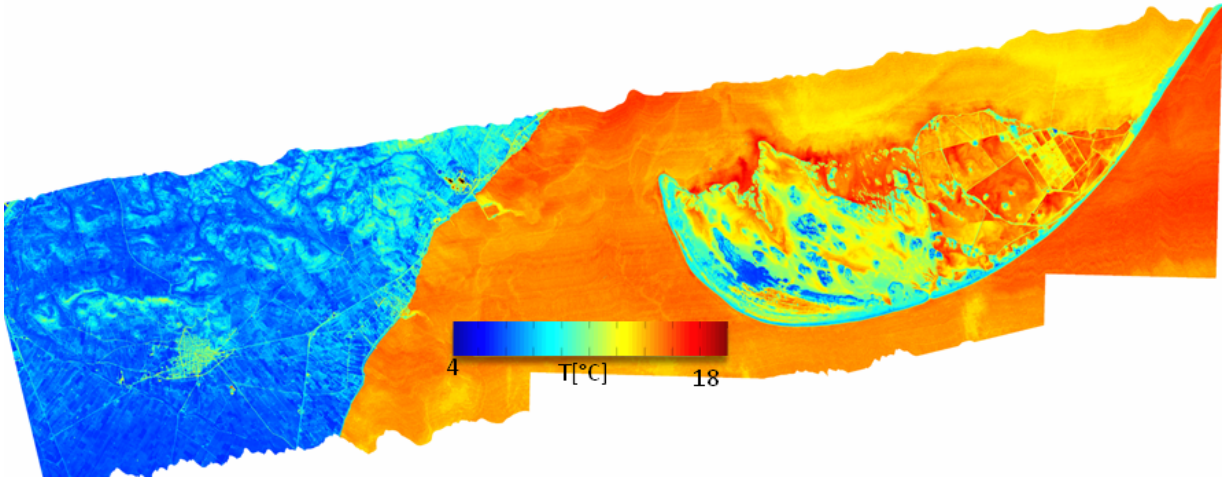

(b)

Figure 6: Ortophoto image (a) from Google Earth of *La Banya* spit, at the south end of the Ebro Delta, and corresponding temperature mosaic (b) obtained from TASI hyperspectral data acquired on 11/03/2010 using ARTEMISS technique.

4- Natural Environment Analysis

Flights with TASI sensor were carried out by ICC in the areas of Delta del Ebre river, in south Catalonia, on March, 11 2010. Data sets were acquired at two different heights: 1600m and 3200m, providing images with a pixel size of 2m×2m and 4m×4m, respectively. Estimation of the atmospheric parameters in the TIR region was carried out using the mid-latitude winter model of MODTRAN5.0 and atmospheric temperature, pressure and relative humidity vertical profiles retrieved by the on-line Atmospheric Correction Parameter Calculator described in [5]. Hyperspectral data were processed as explained in Section 2. The geocoded temperature map retrieved by ARTEMISS corresponding to the spit known as *la Banya* (Figure 6a), at the south end of the Ebro Delta, is shown as example in Figure 6b. Details concerning the three acquisitions necessary to cover the whole area are reported in Table 3. Briefly, the complex temperature patter in the seawater areas are due to cold water fluxes from the land. Contrarily, color variations in the spit are due to the heterogeneity of this natural environment, which is made up of short vegetation, muddy and bare and salted soil areas.

In order to perform an assessment of TASI hyperspectral acquisitions, *in-situ* measurements were carried out in the framework of a collaboration between the ICC and the Universitat de València- Estudi General (UVEG). In this work, two test-areas labeled as Sea Water and Salted Soil areas are analyzed. The location within the area of interest is indicated by the two pins in Figure 6a whereas two photos describing how they looked like from the ground-level are shown Figure 6. Field measurements were acquired during TASI passage using two multiband field radiometers: CIMEL CE 312-1 (4 Channels) and CIMEL CE312-2 (6 Channels) that were employed for sea water and soil, respectively. Absolute ground temperature information was obtained by averaging the values retrieved by inverting the Planck's equation from each band with the emissivity values given by the TES technique [6]. The time-evolution of temperature mean-values retrieved from the ground measurements is displayed in Figure 8. Error bars are the standard deviations in temperature estimation among the different channels of the hand-held radiometers.

Day	Acquisitions	Time	Pixel Resolution	Integration Time
11/03/2010	De15_K1n_T002f12.rf	19:03	4m × 4m	0.34
11/03/2010	De10_K1p_T002f13.rf	19:17	4m × 4m	0.34
11/03/2010	De17_K1n_T002f14.rf	19:29	4m × 4m	0.34

Table 3: Set of TASI data over *La Banya* spit acquired on 11 March 2010.

Figure 8: Salted soil (down) and sea water (up) areas chosen for the in-situ measurements.

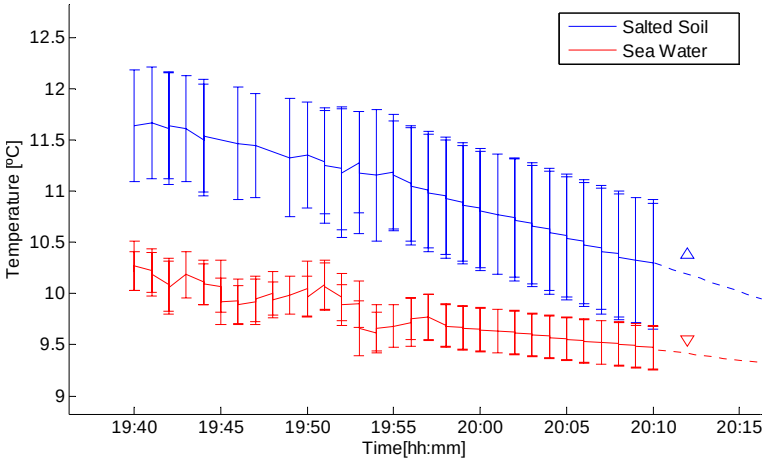

Figure 9: Time evolution of *in-situ* mean temperature and standard deviation versus TASI estimation (data set De10_K1p_T002f13.rf) concerning the salted soil and sea water areas. Dotted lines are extrapolations of *in-situ* curves.

In order to reduce geometrical errors between the retrieved temperature map and *in-situ* measurements, an area around field-GPS measurement was averaged for the TASI-based estimation. The outcome is represented by the red and blue triangles. The time gap between ground-truth and TASI retrieval is due to a delay on the flight-scheduling occurred during the acquisition process that could not be communicated to the on-the-ground group and led eventually to a synchronization mismatch. Yet, the regular temperature trend found for the two areas made it possible to extrapolate the information during the 3 minutes successive to the last measurement and to assess the accuracy of the information extracted from TASI hyperspectral data. It can be observed a fairly good matching between the two estimations, with a maximum error of 0.2 K for the salt soil zone (0.12K for the sea water).

5-Conclusions and Future Work

The study presented in this work constitutes a demonstration of the quality of hyperspectral data acquired by the TASI sensor. The matching between TASI-based temperature estimations and ground-truth measurements for the two cases of nocturnal flights over Barcelona and acquisitions over the test-site of *La Banya* showed that a temperature error in the order of 0.2 K or even lower is achievable. The importance of these results is twofold. On the one hand, they represent a quantitative assessment of the accuracy of the processing chain implemented by ICC for absolute temperature retrievals. On the other hand, they give support to any bio-physical parameter quantitative estimation based on TASI hyperspectral information. For instance, techniques aiming at quantifying evaporation/transpiration processes of natural surfaces are based on the retrieval of energy fluxes which are strictly related to surface skin-temperature. This piece of information, when correlated with vegetation coverage VNIR descriptors, makes it possible to describe the crops water requirements and to detected potential water stress conditions. Future ICC investigations will deal with this issue, in an attempt of combining the hyperspectral thermal information of TASI with the estimation of hyperspectral reflectivity in the VNIR spectrum that CASI sensor, owned by the ICC [7], is able to provide.

References

[1] Itres© Company: http://www.itres.com/Home

[2] Borel, C. 2003, ARTEMISS-an Algorithm to Retrieve Temperature and Emissivity from Hyper-Spectral Thermal Image Data, 28th Annual GOMACTTech Conference, Mar. 31-Apr.3, Tampa, Florida.

[3] Borel, C. 2008, Error analysis for a temperature and emissivity retrieval algorithm for hyperspectral imaging data, *International Journal of Remote Sensing*, No. **17-18**, Vol. **29**, 239-246.

[4] Berk A. at al.. 2005, MODTRAN 5: A Reformulated Atmospheric Band Model with Auxiliary Species and Practical Multiple Scattering Options: Update, *Proceedings of the SPIE*, Vol. **5806**, pp. 662-667.

[5] J.A. Voogt and T.R. Oke, “Thermal Remote Sensing of Urban Climates,” Remote Sensing of Environment, No. 86, 2003, pp. 370-384.

[6] Xarxa d’Estacions Meteorològiques Automàtiques (XEMA) : http://www.meteo.cat/xema/

[7] J.A.Sobrino at al., “DESIREX 2008: Urban Heat Island Analysis in the City of Madrid,” Revista de Teledetección, ISSN: 1988-8740,2009, Vol. 31, pp. 80-92.

[8] Barsi, J.A., J.L. Barker, J.R. Schott, “An Atmospheric Correction Parameter Calculator for a Single Thermal Band Earth-Sensing Instrument,” IGARSS03, Centre de Congres Pierre Baudis, 21-25 July 2003, Toulouse, France.

[9] Gillespie, A.R., S. Rokugawa, T. Matsunaga, J.S. Cothern, S. Hook, and A.B. Kahle, “Temperature and Emissivity Separation from Advanced Spaceborne Thermal Emission and Reflection Radiometer (ASTER) images”, Transaction of Geoscience and Remote Sensing, Vol. 35, No. 4, pp.1113-1126

[10] Martínez L. Arbiol R. y Pérez F. (2010): ICC experiences on DMC radiometric calibration. International Calibration and Orientation Workshop EuroCOW 2008. Castelldefels, 10–12 February.